U.S. ARMY

RESEARCH LABORATORY

Wave Turbine Analysis Tool Development

Gerard E. Welch
U.S. Army Research Laboratory, Lewis Research Center, Cleveland, Ohio

Daniel E. Paxson
Lewis Research Center, Cleveland, Ohio

19980714 048

DTIC QUALITY INSPECTED 1

Since its founding, NASA has been dedicated to the advancement of aeronautics and space science. The NASA Scientific and Technical Information (STI) Program Office plays a key part in helping NASA maintain this important role.

The NASA STI Program Office is operated by Langley Research Center, the Lead Center for NASA's scientific and technical information. The NASA STI Program Office provides access to the NASA STI Database, the largest collection of aeronautical and space science STI in the world. The Program Office is also NASA's institutional mechanism for disseminating the results of its research and development activities. These results are published by NASA in the NASA STI Report Series, which includes the following report types:

- TECHNICAL PUBLICATION. Reports of completed research or a major significant phase of research that present the results of NASA programs and include extensive data or theoretical analysis. Includes compilations of significant scientific and technical data and information deemed to be of continuing reference value. NASA's counterpart of peer-reviewed formal professional papers but has less stringent limitations on manuscript length and extent of graphic presentations.

- TECHNICAL MEMORANDUM. Scientific and technical findings that are preliminary or of specialized interest, e.g., quick release reports, working papers, and bibliographies that contain minimal annotation. Does not contain extensive analysis.

- CONTRACTOR REPORT. Scientific and technical findings by NASA-sponsored contractors and grantees.

- CONFERENCE PUBLICATION. Collected papers from scientific and technical conferences, symposia, seminars, or other meetings sponsored or cosponsored by NASA.

- SPECIAL PUBLICATION. Scientific, technical, or historical information from NASA programs, projects, and missions, often concerned with subjects having substantial public interest.

- TECHNICAL TRANSLATION. English-language translations of foreign scientific and technical material pertinent to NASA's mission.

Specialized services that complement the STI Program Office's diverse offerings include creating custom thesauri, building customized data bases, organizing and publishing research results . . . even providing videos.

For more information about the NASA STI Program Office, see the following:

- Access the NASA STI Program Home Page at *http://www.sti.nasa.gov*

- E-mail your question via the Internet to help@sti.nasa.gov

- Fax your question to the NASA Access Help Desk at (301) 621-0134

- Telephone the NASA Access Help Desk at (301) 621-0390

- Write to:
  NASA Access Help Desk
  NASA Center for AeroSpace Information
  7121 Standard Drive
  Hanover, MD 21076

NASA/TM—1998-208485

ARL–TR–1740

AIAA–98–3402

U.S. ARMY

RESEARCH LABORATORY

Wave Turbine Analysis Tool Development

Gerard E. Welch
U.S. Army Research Laboratory, Lewis Research Center, Cleveland, Ohio

Daniel E. Paxson
Lewis Research Center, Cleveland, Ohio

National Aeronautics and
Space Administration

Lewis Research Center

July 1998

Available from

NASA Center for Aerospace Information
7121 Standard Drive
Hanover, MD 21076
Price Code: A03

National Technical Information Service
5287 Port Royal Road
Springfield, VA 22100
Price Code: A03

Wave Turbine Analysis Tool Development

Gerard E. Welch[*] and Daniel E. Paxson[†]

NASA Lewis Research Center, Cleveland, OH

A quasi-one-dimensional (Q-1-D) computational fluid dynamic solver, previously developed and validated for pressure-exchanger wave rotors, is extended in the present work to include the blade forces of power producing wave rotors (*i.e.*, wave turbines). The accuracy of the single-passage Q-1-D solver is assessed relative to two two-dimensional solvers: a single-passage code and a multi-block stator/rotor/stator code. Comparisons of computed results for inviscid, steady and unsteady flows in passage geometries typical of wave rotors reveal that the blade force model is accurate and that the correlation (effective stress and heat flux) terms of the Q-1-D passage-averaged formulation can be neglected. The ends of the rotor passages pose particular challenges to Q-1-D formulations because the flow there must at times deviate significantly from the mean camber line angle to match the port flow fields. This problem is most acute during the opening and closing of the rotor passages. An example sub-model is developed to account for the deviation between the flow departure angle and the mean camber line exit angle that occurs as an inviscid flow decelerates to meet a uniform pressure boundary. Comparisons of results from four-port wave turbine simulations reveal that the Q-1-D solver currently overpredicts wave turbine performance levels and highlight the need to devote future effort to the boundary conditions and sub-models of the Q-1-D solver.

Nomenclature

a = $(\gamma p / \rho)^{1/2}$, local speed of sound

e_i = $h_i - p / \rho$, rothalpic energy

F^B = blade force source term (Eqn. 2)

F^C = momentum correlation source term[12]

h_i = $\gamma p / ((\gamma-1)\rho) + \frac{1}{2} u \cdot u - u_\theta r \Omega$, specific rothalpy

L^P = rotor blade pitch

p = static pressure

Q^C = passage-averaged effective heat flux term[12]

R = (R, μ), blade polar coordinates (Fig. 12)

r = (x, θ, r), position vector (absolute ref. frame)

S = $\iint r \, d\theta \, dr$, passage cross-sectional flow area

t = time

u = $(u_x, u_\theta, u_r [= 0])$, fluid absolute velocity

α_m = nondimensional mass flow rate

α_e = nondimensional total enthalpy flow rate

β = $\tan^{-1}([u_\theta - r\Omega]/u_x)$, relative swirl angle

δ^2 = $1 + \overline{\tan\beta}^2 + \overline{\tan\phi}^2$, "blockage" term

δ^D = flow deviation at rotor passage exit

γ = ratio of specific heats

η^e = exhaust process polytropic efficiency (Eqn. 3)

κ = $\frac{1}{2}\overline{u' \cdot u'} - \overline{u'_\theta (r\Omega)'}$, nonuniformity kinetic energy

ρ = mass density

σ = ratio of blade chord to pitch (*i.e.*, solidity)

ϕ = $\tan^{-1}(u_r/u_x)$, meridional flow angle

Ω = angular speed

Special symbols

$\overline{}$ = passage-averaged value

$\overline{\overline{}}$ = density-weighted passage-averaged value

$'$ = deviation from the density-weighted passage-averaged value

Δ = $\Delta(\psi) \equiv \psi_T - \psi_H$, spanwise difference

Δ^r_θ = $\Delta^r_\theta(\psi) \equiv \psi_P - \psi_S$, pitchwise difference

Subscripts

0 = stagnation property

1 = initial uniform passage condition (Fig 1)

2 = rotor/exhaust-port interface plane (Fig. 1)

3 = exhaust-port exit plane (Fig. 1)

C = rotor blade mean camber line trailing edge

ex = four-port wave rotor low pressure exhaust port

in = four-port wave rotor low pressure inlet port

m = mixed-out exhaust-port value

H = rotor hub

P = rotor passage leading blade surface

S = rotor passage trailing blade surface

T = rotor tip-shroud

Introduction

Wave rotors are members of the family of dynamic pressure exchange devices.[1] The wave rotor family includes pressure-exchangers and wave turbines. Pressure-exchangers have uncambered, axially aligned blades and produce negligible shaft power (*e.g.*, see Ref. 2). Wave turbine blades are designed to induce absolute flow turning and thus produce net shaft power.[3,4] Wave

1

rotor topping offers the potential to improve the performance levels of gas turbine engines significantly, within the constraints of current material temperature limitations.[5] Recent studies indicate that topping with a wave turbine may afford more significant enhancement of engine specific power levels than does pressure-exchanger topping.[6,7] These studies assumed that gasdynamic waves propagate along the wave turbine passages according to one-dimensional gasdynamic theory (cf. Ref. 8). The accuracy of this assumption remains to be assessed. Further, in spite of the potential merits of wave turbine topping, most of the recent CFD-based wave rotor tools have been developed to simulate the geometrically simpler pressure-exchangers (*e.g.*, Refs. 9-11). It is necessary to develop one-dimensional design/analysis tools which are able to simulate the flow in wave turbine rotor geometries efficiently and accurately.

The purpose of the work presented herein was twofold: first, to incorporate the blade force model developed in Ref. 12 into the quasi-one-dimensional (Q-1-D) design/analysis code of Ref. 9 in order to extend its applicability to include wave turbines; second, to assess the accuracy of the blade force model by comparing predictions by the modified Q-1-D code with time-averaged numerical data from a two-dimensional (2-D) multi-block (stator/rotor/stator) code.[13,14]

The 2-D multi-block computational results, reported herein and elsewhere,[14] have revealed strong gasdynamic interaction between the rotor and port flow fields. This interaction is typically neglected in single-passage codes (*e.g.*, see Refs. 9 and 11) which use constant and uniform boundary conditions. However, consider the instantaneous static pressure contours in the wave rotor exhaust port shown in Fig. 1. The evident flow field unsteadiness is sustained by compression waves which are emitted from the rotor as each rotor passage gradually opens to the exhaust port. To account for this interaction fully, a single-passage code would necessarily employ time-varying boundary conditions to simulate the unsteadiness in the duct flow fields; however, to specify such a boundary condition would require knowledge of the desired solution. A compromised improvement over a uniform boundary condition is a constant, nonuniform boundary condition which better simulates the time-mean exhaust port flow field (see Fig. 1). In the event that a constant (time-mean), uniform (tangentially averaged) boundary condition is used to simulate the port flow field, it should account for the gasdynamic interaction between the rotor and port flow fields.

The gasdynamic interaction is sufficiently strong in the scenarios considered in this work that the root causes of disparities between the modified Q-1-D single-passage and 2-D multi-block numerical results are obscured. A step-wise approach to assess the accuracy of the Q-1-D code is therefore adopted. The Q-1-D blade force model[12] is first validated by comparing the Q-1-D single-passage code results with those of a 2-D *single-passage* code, for both steady and unsteady flows. The 2-D single-passage code uses the same numerical methods as the multi-block solver (see Ref. 13) but is subject to the same constant boundary conditions imposed in a Q-1-D calculation. The accuracy of the two (Q-1-D and 2-D) single-passage codes is then assessed relative to the 2-D multi-block code.

The flow is considered to be inviscid in the present work. Modification and re-validation of the Q-1-D viscous force source term of Ref. 9 is beyond the scope of the current effort and remains for future work.

The paper is arranged as follows: the Q-1-D and 2-D solvers are first described. The Q-1-D blade force model is then evaluated by comparing results from the Q-1-D and 2-D solvers, for steady and unsteady flow problems, in passage geometries typical of optimized pressure-exchanger and wave turbine rotors (cf. Refs. 7 and 8). A four-port wave turbine is simulated and results from the Q-1-D single-passage code and 2-D multi-block code are compared. Planned future work is outlined in the summary. In the appendix, a model is developed for predicting the deviation between the flow departure angle and the exit angle of the mean camber line for an inviscid flow.

Computational Models

Quasi-One-Dimensional Single-Passage Solver

Quasi-one-dimensional (Q-1-D) passage-averaged equations for an Euler flow in arbitrary wave rotors geometries were developed in Ref. 12. In the present work, these equations are applied at a constant mean radius about which the hub and the tip shroud are symmetric (*i.e.*, $\overline{\tan\phi} = 0$) and thus take the form

$$\frac{\partial}{\partial t}\begin{bmatrix} \overline{\rho}S \\ \overline{\rho}\,\overline{\overline{u}}_x S\,\delta^2 \\ \overline{\rho}\,\overline{\overline{e}}_i S \end{bmatrix} + \frac{\partial}{\partial x}\begin{bmatrix} \overline{\rho}\,\overline{\overline{u}}_x S \\ \overline{\rho}\,\overline{\overline{u}}_x \overline{\overline{u}}_x S\,\delta^2 + \overline{p}S \\ \overline{\rho}\,\overline{\overline{u}}_x \overline{\overline{h}}_i S \end{bmatrix} = \begin{bmatrix} 0 \\ F_B + F_C \\ Q_C \end{bmatrix} \quad (1)$$

where the overbar denotes an unweighted passage-average and the double overbar denotes a density-weighted passage-average. The local static pressure is

Table 1. Comparison between Q-1-D and 2-D single-passage solutions of steady-state, inviscid flow in circular-arc passages with zero-degree inlet blade angle ($\gamma = 1.4$, $(p/p_0)_{ex} = 0.843$).

Parameter	Quasi-one-dimensional				Two-dimensional			
	$-30°$ exit		$-70°$ exit		$-30°$ exit		$-70°$ exit	
	Inlet	Exit	Inlet	Exit	Inlet	Exit	Inlet	Exit
Static pressure (p/p_0)	0.890	0.845	0.984	0.855	0.887	0.843	0.981	0.851
Mach number	0.424	0.511	0.156	0.491	0.418	0.500	0.165	0.488
Swirl angle	0.0	-29.3*	0.0	-66.7*	0.0	-29.3	-0.315	-68.0

*Post-processed with the deviation model described in the appendix.

$\bar{p} = (\gamma - 1)\bar{\rho}\,(\bar{e}_i - \frac{1}{2}\overline{u_x}\,\overline{u_x}\delta^2 + \frac{1}{2}(\bar{r}\Omega)^2 - \kappa)$ and the local specific rothalpy is $\bar{h}_i = \bar{e}_i + \bar{p}/\bar{\rho}$. In the limit of $\overline{\tan\phi} = 0$, the blockage term is $\delta^2 = 1 + \overline{\tan\beta}^2$ and the first momentum source term is

$$F_B = \frac{\bar{\rho}\,\overline{u_x}\,\overline{u_x}\,S}{2}\frac{\partial \delta^2}{\partial x} + \bar{p}S\left[\frac{\Delta_\theta(\tan\beta)}{\bar{r}(\theta_P - \theta_S)} + \frac{\Delta_r(\tan\phi)}{r_T - r_H}\right] \quad (2)$$

The source terms F_C and Q_C are passage-average "stress" and "heat flux" terms and were discussed in detail in Ref. 12; they contain correlation terms that arise by expanding the passage-averages of variable products into the passage-averaged variables.

Equation 1 is a set of quasi-one-dimensional equations in which the source term F_B (Eqn. 2) accounts for the influence of blade, hub, and tip-shroud profiling on the rotor flow. Note that by applying Eqn. 1 under the additional restrictions of constant-radius hub and tip-shroud surfaces with uncambered constant thickness blades at stagger (i.e., $\delta^2 = 1/\cos^2\beta$ and $F_B = 0$), a conservative form of the equations is recovered. Further, the classical quasi-one-dimensional equations in which the walls are symmetric about a mean flow line are recovered in the limiting case of $\delta^2 = 1$ and $\overline{\tan\phi} = \overline{\tan\beta} = 0$.

The force integral term F_B (Eqn. 2) was implemented in the Q-1-D wave rotor code[9] in the manner previously described for area-variation.[15] The boundary conditions are specified so as to properly account for the kinetic energy invested in the local non-axial velocity components which are obtained, according to the Q-1-D passage-averaged formulation,[12] from $\overline{u_\theta} \equiv \overline{u_x}\,\overline{\tan\beta} + \bar{r}\Omega$ and $\overline{u_r} \equiv \overline{u_x}\,\overline{\tan\phi}$.

Two-Dimensional Solvers
The numerical data from the Q-1-D solver are compared in this paper with computed data from the two (single-passage and multi-block) 2-D (x, θ) solvers. The single-passage 2-D code simulates the flow dynamics in a wave rotor passage as it moves past the various ports and endwalls. The ports are simulated by constant, uniform boundary conditions. The multi-block code simultaneously simulates the flow field in multiple passages and multiple inlet and exhaust ports. Both 2-D codes use the numerical methods described in Refs. 13 and 14. All computations in this work are inviscid and are carried out at mid-span (i.e., at $\bar{r}$). The numerical data from the 2-D multi-block code presented herein are obtained by time averaging the local unsteady flow over one blade passing period during which the flow in the wave rotor is assumed to be periodic. This assertion was validated by comparing time-averages over one, three, and eleven blade passing periods.

Steady-State Flow in a Stationary Passage
As a preliminary check of the blade force model proposed in Ref. 12, the Q-1-D and 2-D single-passage solutions of steady-state, inviscid flow through a passage defined by identical circular arcs are compared. The correlation terms, κ, F_C, and Q_C, are neglected. The inlet blade angle is zero degrees in both cases. Two outlet blade angles are considered: negative thirty degrees and negative seventy degrees. The blades are separated at each axial location by a distance equal to one-tenth the arc length (i.e., $\sigma = 10$). The inlet total pressure and total enthalpy are specified as uniform and constant. A uniform and constant back pressure is specified at 0.843 times the inlet total pressure for the $\gamma = 1.4$ flow. Important inlet and outlet flow field values are compared in Table 1. The Q-1-D and 2-D steady-state solutions agree well. By comparing the $-30°$ and the $-70°$ cases, it is evident that the disparity between the Q-1-D and 2-D results increases as the camber angle increases. Possible sources of error include deficiencies in the blade force model and the unmodeled correlation terms; still, for engineering analysis purposes, the Q-1-D blade force model adequately describes the steady flow field in both

geometries. It is concluded that the blade-to-blade correlation terms are indeed negligible for these steady-state flow calculations in the passage geometries considered here. It is also noted from the 2-D results that the flow is discharged from the rotor passage with some deviation from the exit angle of the mean-camber-line. A sub-model for predicting this deviation angle in an inviscid flow is developed in the appendix and is used to enhance the accuracy of the Q-1-D computations reported in this work. The sub-model is implemented by post-processing the Q-1-D results rather than by modifying the prescribed blockage (δ^2) profile in the present study.

Wave Rotor Exhaust-Port Problem

Problem Description

Consider a wave rotor passage containing high pressure, high temperature gas at rest relative to the spinning rotor as shown in Fig. 1. Initially, the gas is contained by the casing endwalls to which the rotor flow annuli are exposed (state 1). As a rotor passage opens to the exhaust-port shown, an expansion wave propagates into the rotor passage and expands the on-board gas out into the exhaust-port. A compression wave is emitted from the rotor into the exhaust port as each rotor passage opens. The exhaust-port discharge process is critical to wave rotors of the type considered for gas turbine engine topping cycles. This process can be characterized by the fractions of mass and energy initially in the rotor passage which are discharged to the port and by the efficiency of the discharge process.[8] The expansion process itself is 100% efficient in the present study because the flow is inviscid; however, the expansion fan effects a highly nonuniform flow field which, in practice, will mix-out via diffusion to some uniform state of higher entropy. The efficiency of the discharge/mixing process can be gauged by an effective polytropic efficiency obtained by relating the mixed-out properties in the exhaust-port, just downstream of the rotor/port interface (state m at position 2), to the uniform properties initially in the rotor (state 1):

$$\eta_e \equiv \frac{\gamma}{\gamma-1} \frac{\log_e (h_{0,m}/h_{0,1})}{\log_e (p_{0,m}/p_{0,1})} \qquad (3)$$

While neglecting all modes of entropy production except that due to mixing the nonuniform flow field, it is found analytically that the polytropic efficiency of this discharge/mixing-out process can be as low as 94% in pressure-exchangers.[8] Because of the importance of this discharge process to machine performance, and the ability to isolate this process from the remainder of the wave diagram (as done in Fig. 1), the exhaust-port

discharge problem is used as a test case to compare the Q-1-D and 2-D results. The strength of the expansion fan is dictated by the ratio of the uniform, constant static pressure at position 2 to the initial static pressure on-board the rotor (state 1).

Three wave rotor geometries are considered in this study: a.) a pressure-exchanger with uncambered blades at $0°$ stagger angle (i.e., axially aligned); b.) a wave turbine with uncambered blades at $-45°$ stagger angle; and c.) a wave turbine with symmetric circular-arc blades with $60°$ camber angle at $0°$ stagger angle. The hub and tip-shroud are constant radius surfaces in all cases. Pertinent nondimensional geometry and speed parameters for the simulations are summarized in Table 2. The rotor blades have zero thickness so that blade-blockage-effects do not obscure the comparisons. The discharge problem described above is analyzed for each rotor geometry by using the Q-1-D code, the 2-D single-passage code, and the 2-D multi-block code. The Q-1-D and 2-D single passage computations are carried out with a constant, uniform static pressure ($p_2 = 0.4 p_1$) imposed at the rotor/exhaust-port interface (position 2 of Fig 1). The 2-D multi-block computations are carried out by imposing the same static pressure, constant and uniform, at the duct exit (position 3 of Fig. 1) while allowing the static pressure at position 2 to develop in space and time. The duct walls are parallel in the 2-D multi-block computation so that the flow is not decelerated by area variation.

Comparisons of Computed Flow Variable Profiles and Discharge Process Performance

Pressure-exchanger with unstaggered, uncambered blades. The axial and tangential velocity profiles predicted by the three solvers for the exhaust port of a pressure-exchanger are compared in Figs. 2 and 3. The two (Q-1-D and 2-D) single-passage predictions agree well. This comparison indicates the level of agreement which is to be expected for inviscid flow computations and should be obtained in the wave turbine cases (below) in which the blade forces are non-zero. The evident discrepancy between the single-passage computations and the 2-D multi-block computations has three causes—one has to do with a difference in the positions at which the data are computed and two are deficiencies in the boundary conditions imposed on the single-passage computations. First, the velocities of the single-passage computations are instantaneous values in the rotor, one computational cell upstream of the rotor/duct interface. The multi-block results are time-averaged values assessed in the port, one computational cell downstream of the rotor. As the rotor passages open to the exhaust port, gas is discharged in a jet of high velocity. Although the (port) jet velocity is high,

4

Table 2. Wave rotor geometry data and computed performance results of model exhaust port problems ($\gamma = 1.315$).

Parameter		Pressure-exchanger	WT-stagger	WT-circular-arc
Passage opening time ($a_1/(r\Omega\sigma)$)		0.476	0.214	0.214
Passage aspect ratio (σ)		14	10	10
Nondimensional rotor speed ($r\Omega/a_1$)		0.15	0.467	0.467
Inlet blade angle, degrees		0	-45	+30
Exit blade angle, degrees		0	-45	-30
Mass discharge fraction(α_m)	Q-1-D	0.6504	0.4694	0.6158
	2-DSP	0.6575	0.4692	0.6178
	2-DMB	0.6561	0.4749	0.6291
Energy discharge fraction(α_e)	Q-1-D	0.5658	0.3807	0.5143
	2-DSP	0.5710	0.3816	0.5166
	2-DMB	0.5725	0.3857	0.5245
Expansion/mixing efficiency, %	2-DMB	0.9637*	0.9735	0.9704

*The pressure-exchanger expansion/mixing efficiency predicted by the Q-1-D solver is $\eta^e = 0.954$.

the passage-averaged value of velocity inside, at the opening end, of the rotor passage gradually rises from zero to a maximum when the passage is fully open. Second, in the same (leading) end of the duct the gasdynamic interaction caused by the compression waves emitted into the exhaust port as the rotor passages gradually open (see Fig. 1) is not simulated by the constant and uniform single-passage boundary conditions. The time-mean static pressure at the rotor/port interface is nonuniform as shown in Fig. 4: the circumferentially-mass-averaged time-mean static pressure at position 2 is slightly higher than the uniform static pressure boundary condition of the single-passage calculations. The time-mean tangential pressure gradient of Fig. 4 is consistent with the lower axial velocities computed by the 2-D multi-block code (see Fig. 2). Note, however, that the mass flow rates predicted by the single-passage and the multi-block solvers are nearly the same (see Table 2). In general, the instantaneous, and hence the time-mean, static pressure distribution will be influenced further by the exhaust duct geometry. Third, the ends of the rotor pose particular challenges in that the influence of the port flow field can act to misalign the passage-averaged rotor flow from the mean camber line. The rotor flow field is significantly influenced by the gasdynamic waves that enter the rotor during the passage opening and closing processes. The waves can influence the relative flow field as much as or more than the blades do during these processes. This highlights the need for sub-models to predict the relative flow

angle accurately during passage opening and closing. As mentioned earlier, even when a passage is fully opened, flow deviation can occur in the uncovered portions of the rotor as the flow adjusts to meet the exit back pressure at the rotor/exhaust-port interface (see the appendix). In spite of the disparities attributed to the deficiencies in the specified single-passage boundary conditions, the results from the single-passage and multi-block solvers are in good agreement. The mass and energy discharge fractions computed by the three solvers are in very good agreement (see Table 2).

Wave turbine with staggered, uncambered blades. The axial and tangential velocity profiles are compared in Figs. 5 and 6 for the exhaust port of a wave turbine with uncambered blades at -45° stagger. As expected, the chordwise (total) velocity is the same as the axial velocity of the pressure-exchanger: the impact of the stagger is essentially to reduce the theoretical value of axial velocity by a factor of $\cos(45°) = 1/\sqrt{2}$. The corresponding theoretical value of the tangential velocity component ($\overline{\overline{u_\theta}} = \tan\beta\,\overline{\overline{u_x}} + \overline{\overline{r\Omega}}$) is, by design, nearly zero following the passage opening process. The Q-1-D and 2-D single-passage results show excellent agreement and indicate that the passage-averaged correlation terms associated with local pitchwise flow field nonuniformities are negligible; that is, the correlation terms established by local acceleration induced by the expansion fan (*i.e.*, relative unsteadiness[12]) are negligible in the uncambered geometry in which there is no

5

relative flow turning. Again, the discrepancy between the single- and multi-block codes points to the deficiency in the uniform static pressure boundary condition employed in the Q-1-D code and not to a deficiency in the blade force model of Ref. 12. Specific total enthalpy profiles are compared in Fig. 7. The agreement is good; following the passage opening transient (here between 0 and 10% of port-width), the two single-passage codes show nearly identical behavior and follow the multi-block results very closely. This indicates that the rotor produces essentially the same power during the exhaust port discharge process. The discharge metrics are again found to be in very good agreement (see Table 2).

Wave turbine with circular-arc, unstaggered blades. Comparisons of the axial and tangential velocity profiles predicted by the three CFD solvers for the exhaust port of a wave turbine with unstaggered, circular-arc blades are shown in Figs. 8 and 9. Specific total enthalpy profiles are compared in Fig. 10. The inlet and exit blade angles are +30-degrees and -30-degrees, respectively. The 60-degree camber angle is conservatively chosen to be larger than optimized wave turbine geometries propounded in Ref. 7. The Q-1-D and 2-D single-passage codes again show excellent agreement. Note that the subtle convexity in the axial velocity profile is reproduced by the Q-1-D code. This agreement further validates the blade force model and its implementation in the Q-1-D code. It is again inferred that the correlation terms associated with pitchwise nonuniformities—here established by flow acceleration induced by relative unsteadiness (the expansion waves) and relative flow turning—are relatively small. Consistent with the earlier results (Figs. 2 and 5), there is significant discrepancy between the single-passage and multi-block solutions during the passage opening (here between 0 and 10% of port-width), primarily due to the difference between observing in the passage and in the port. The disparity persists after the passage opening transient due to the finite tangential pressure gradient in the exhaust port which is not modeled adequately by the uniform back pressure imposed in the single-passage computations. The mass and energy discharge fractions computed by the three solvers agree well (see Table 2).

Implications of Agreement
Results from the Q-1-D and 2-D single-passage codes agree very well. It is concluded, therefore, that the Q-1-D formulation suggested in Ref. 12 can be used to simulate accurately the unsteady flow fields in axial wave turbine rotors with hub and tip-shroud surfaces of constant radius and with blades of zero thickness. The accuracy is obtained without modeling the correlation

terms of the passage-averaged description in the simple geometries considered.

The rotor passage ends pose a particular challenge to the Q-1-D model. The port flow fields can significantly impact the rotor flow field, especially during the passage opening and closing processes. In practice, the modeler must augment the Q-1-D flow description at the rotor passage ends with sub-models that account for flow incidence and deviation. This challenge is common to modeling pressure-exchangers and wave turbines.

Wave Turbine Performance Comparison
A four-port through-flow wave turbine[7] has been simulated using the modified Q-1-D solver and the 2-D multi-block solver. The wave turbine has two low pressure (LP) ports and two high pressure (HP) ports (see Fig. 11). High temperature, high pressure gas is discharged by an expansion wave from the rotor to the low pressure exhaust port while fresh air is ingested through the low pressure inlet port. The high pressure exhaust port carries a mixture of fresh air and gas to an external burner (not shown) while the high pressure inlet port ingests the burner discharge. The rotor has an inlet blade angle of $0°$ and an outlet blade angle of $-30°$. The ratio of specific heats is $\gamma = 1.4$, the passage solidity is $\sigma = 10$, and the normalized rotor speed (rotor Mach number) is $\bar{r}\Omega/a_{0,in} = 0.6894$. The applied boundary conditions assure that the following parameters are the same for both computations: the ratio of the absolute total enthalpies in the two low pressure ports; the ratio of mass flow rate through the high pressure ports to the mass flow rate through the low pressure ports; and the ratio of the static pressure at the rotor/low-pressure-exhaust port interface to the absolute total pressure in the inlet port. The inlet flow angles of the Q-1-D computation are set at the inlet duct angles. Post-processing tools are used to assure that the other Q-1-D boundary conditions simulate the time-mean, tangentially averaged conditions at the rotor face as computed by the 2-D code. This helps to account for the impact of the gasdynamic interaction between the port and rotor flow fields. Important wave turbine variables are summarized in Table 3.

Surprisingly, the specific power predicted by the Q-1-D solver is 25% higher than the 2-D solver prediction; further, the engine efficiency (*i.e.*, the ratio of wave rotor shaft power to external burner heat addition) predicted by the Q-1-D solver is 14.3% which is significantly higher than the 11.8% predicted by the 2-D solver. The predicted burner pressure drop fractions differ significantly as well (see Table 3). The differences are not within the accuracy required for analysis tools

6

Table 3. Comparison of computed results for four-port through-flow wave turbine with circular-arc blades at $0°$ inlet and $-30°$ exit ($\gamma = 1.4$, $\bar{r}\Omega/a_{0,in} = 0.6894$, $\sigma = 10$).

Parameter	Q-1-D[a]	Q-1-D[b]	2-D
Total enthalpy ratio ($h_{0,ex}/h_{0,in}$)	2.061	2.061	2.061
Total pressure ratio ($p_{0,ex}/p_{0,in}$)	1.034	1.024	1.017
High-pressure to low-pressure loop mass flow rate ratio	1.662	1.656	1.665
Corrected mass flow rate ($\dot{m}a_{0,in}/(\gamma p_{0,in}A_{in})$)	0.302	0.290	0.286
Burner total pressure drop ($\Delta p_0/p_0$), %	8.0	8.9	4.7
Specific power (shaft-power/($\dot{m}h_{0,in}$))	0.177	0.153	0.142
Engine efficiency (shaft-power/burner-heat-addition), %	14.3	12.6	11.8

[a] inlet flow angles set to duct angle. [b] inlet flow angles set to inlet flow angles computed by 2-D solver.

and are inconsistent with the excellent agreement reported earlier in this paper. The disparities are attributed to two factors. First, the absolute total properties—hence wave rotor shaft power and engine efficiency—are extremely sensitive to the inlet port absolute flow angles. The inlet flow angles must be inferred from the duct geometry in the Q-1-D modeling and are not rigorously known. As shown in Table 3, when the Q-1-D inlet flow angles are set equal to the computed inlet flow angles of the 2-D solver, rather than to the inlet duct angles, the relative error in specific power is reduced to 8% and the difference in engine efficiency is only 0.8%. Second, the flow dynamics of the passage opening processes in the high pressure inlet port adversely redistribute hot and cold flow in the rotor (see Fig. 11 and extensive discussion of such in Ref. 14). Some of the fresh air that is intended for the high pressure exhaust port is discharged to the low pressure exhaust port; similarly, some hot gas intended for the low pressure exhaust port leaves through the high pressure exhaust port. The Q-1-D solver does not currently account for this redistribution. Future effort is required to develop a sub-model for the Q-1-D solver that accounts for this redistribution and its impact on performance.

Summary
The quasi-one-dimensional solver of Ref. 9 was successfully modified to incorporate the blade force term derived in Ref. 12. The simple blades considered in the present study were at constant pitch and had no thickness. The rotor hub and the tip-shroud were each at constant radius. The agreement between the results from the Q-1-D and 2-D single-passage solvers has demonstrated the accuracy of the blade force model for these geometries and has implicitly shown that the correlation terms introduced by passage averaging are small in the wave rotor geometries considered, for

steady and unsteady, inviscid flow fields. It remains for future work to validate the Q-1-D model for more complicated passage geometries; indeed, the Q-1-D formulation offered in Ref. 12 accommodates generalized blade shapes and hub and tip-shroud profiling. The positive experience in validating the blade force model described herein gives confidence that the remaining terms of the general force terms of Ref. 12 can be implemented and validated with equal success.

The comparison of results from the single-passage (Q-1-D and 2-D) codes with results from the 2-D multi-block code showed that the gasdynamic interaction between the rotor and port flow fields significantly impacts the time-mean wave rotor flow field. The boundary conditions imposed on a single-passage code should account for this interaction. For example, the constant and uniform static pressures imposed as outflow boundary conditions at the rotor/exhaust port interfaces should account for the compression waves that are emitted from the rotor passages to the exhaust port during the passage opening processes.

While the Q-1-D solver accurately predicts the axial velocity component, the remaining velocity components are inferred from the prescribed blade mean camber line and the hub and tip-shroud profiles. The ends of the rotor pose a particular challenge: the port flow fields impact the rotor flow field and can misalign the passage-averaged rotor flow relative to the blade mean camber line. In the inlet ports, the absolute flow angles are largely set by the duct walls and in general the flow will attack the rotor blades with negative or positive incidence. In the portions of the exhaust ports in which the passages are fully opened, the flow must adjust to meet a uniform pressure at the rotor/exhaust-port interfaces. The rotor flow field is significantly

influenced by the gasdynamic waves associated with the opening and closing of the rotor passages. Evidently, sub-models for flow incidence and deviation are needed to augment the Q-1-D flow description at the rotor passage ends.

A four-port through-flow wave turbine was simulated with the Q-1-D and 2-D multi-block flow solvers. It was found that the Q-1-D code substantially overpredicted the wave turbine performance levels. The disparities are attributed to incorrectly inferred inlet port flow angles and redistribution of hot and cold gases in the rotor caused by passage opening flow dynamics. The accuracy of Q-1-D wave turbine simulations should be improved by planned development of modified boundary conditions and incidence and deviation sub-models for wave turbines.

Appendix
Deviation Angle Model for Inviscid Flow

An example model for estimating the deviation angle, δ^D, between the mean flow exhausting from a rotor passage and the mean camber line is presented in this appendix. The model is for inviscid flow. A similarly simple model for viscous flow will be needed in practice. The viscous flow model must account for inviscid deceleration needed to satisfy the single-passage boundary conditions and the local behavior of the boundary layer (e.g., displacement thickness evolution and flow separation).

The flow in the uncovered portion of the passage shown schematically in Fig. 12 must adjust to meet a uniform back pressure at the interface of the rotor and the exhaust port. If the blade has curvature at the trailing edge, the static pressure at point 2 (see nomenclature in Fig. 12) is lower than the static pressure at point 1, which is equal to the static pressure at point 3; therefore, a particle decelerates as it moves from point 2 to 3. The local streamlines will diverge as the flow decelerates. This results in a slight positive turning (relative to the mean camber line) of the flow in the uncovered region. The static pressure at the blade surface between points 2 and 3 is $p_2 \leq p(R_2, \mu) \leq p_3$.

Aside from times during which either contact discontinuities or shock waves propagate through the uncovered region, the circulation of the control volume defined by the uncovered region must be constant for an inviscid flow; that is, $\oint u \cdot dl = 0$ where the contour is defined by the boundary of the uncovered region. The flow entering the uncovered region is assumed to be irrotational and in "radial" equilibrium between effective inner (R_2) and outer (R_1) radii which are related by

$$\frac{R_1}{R_2} \approx \frac{1 + \frac{1}{2}\cos\beta_C (L_P/\bar{R}_C)}{1 - \frac{1}{2}\cos\beta_C (L_P/\bar{R}_C)} \qquad \text{(A-1)}$$

The blade pitch (L_P) and the radius of curvature ($\bar{R}_C$) of the mean camber line are set by the rotor geometry. The total properties of the flow entering the control volume are "radially" uniform and the back pressure at the exit plane is uniform; therefore, the total velocity at the exit plane is uniform, although the exit flow angle varies. Integration of the streamwise momentum equation under the assumption that the static enthalpy varies linearly with distance along the inner blade surface yields an expression for the distribution of streamwise velocity ($u_\mu(R_2, \mu)$). The streamwise velocity is used in the circulation conservation constraint

$$\overline{\sin(\beta_C + \delta^D)} \approx -\frac{R_2}{L_P} \int_{\mu_2}^{\mu_3} \frac{u_\mu(R_2, \mu)}{u_{\mu, ex}} d\mu \qquad \text{(A-2)}$$

to approximate the flow deviation as

$$\delta^D \approx -|\tan\beta_C| [sign(\beta_C) + \frac{2}{3} \frac{1 - (2 - (R_1/R_2)^2)^{3/2}}{(R_1/R_2)^2 - 1}] \qquad \text{(A-3)}$$

Note that this expression depends only on the blade geometry. Finally, it is noted that the derived deviation (Eqn. A-3) is well approximated by a more simple expression obtained by assuming that the flow discharges normal to the "throat" of the uncovered region; that is, $\delta^D \approx -\frac{1}{2}(L_P/\bar{R}_C)\sin\beta_C$.

References

[1]Azoury, P.H., *Engineering Applications of Unsteady Flow*, Wiley, New York, 1992.

[2]Kentfield, J. A. C., *Nonsteady, One-Dimensional, Internal, Compressible flows: Theory and Applications*, Oxford University Press, New York, 1993, pp. 125-190.

[3]Weber, H. E., *Shock Wave Engine Design*, Wiley, New York, 1995.

[4]Pearson, R. P., "Performance Predictions for Gas Wave Turbines including Practical Cycles with Wide Speed Range," eds., Shreeve, R. P. and Mathur, A., *Proc. 1985 ONR/NAVAIR Wave Rotor Research and Technology Workshop*, NPS-67-85-008, Naval Postgraduate School, Monterey, CA, 1985, pp. 329-378.

[5]Welch, G. E., Jones, S. M., and Paxson, D. E., "Wave-Rotor-Enhanced Gas Turbine Engines," *J. Engineering for Gas Turbines and Power*, **119**, No. 2, April, 1997, pp. 469-477.

[6]Lear, W. E., Jr. and Kielb, R. P., "The Effect of Blade Angle Design Selection on Wave-Turbine Engine Performance," ASME-96-GT-259, June, 1996.

[7]Welch, G. E., "Wave Engine Topping Cycle Assessment," AIAA-97-0707, Jan., 1997; also NASA TM-107371 and ARL-TR-1284, Dec., 1996.

[8]Welch, G. E., "Macroscopic Balance Model for Wave Rotors," *J. Propulsion and Power*, **13**, No. 4, July-Aug., 1997, pp. 508-516.

[9]Paxson, D. E., "Comparison Between Numerically Modeled and Experimentally Measured Wave-Rotor Loss Mechanisms," *J. Propulsion and Power*, **11**, No. 5, Sept.-Oct., 1995, pp. 908-914.

[10]Paxson, D. E., "A Numerical Simulation of Dynamic Wave Rotor Performance," *J. Propulsion and Power*, **12**, No. 5, Sept.-Oct., 1996, pp. 949-957.

[11]Fatsis, A and Ribaud, Y., "Numerical Analysis of the Unsteady Flow Inside Wave Rotors Applied to Air Breathing Engines," *Proc. of the 13th Int. Symp. on Air Breathing Engines*, **2**, ISABE 97-7214, Sept., 1997, pp. 1537-1547.

[12]Welch, G. E. and Larosiliere, L. M., "Passage-Averaged Description for Wave Rotor Flows," AIAA-97-3144, July, 1997; also NASA TM-107518 and ARL-TR-1462, July, 1997

[13]Welch, G. E. and Chima, R. V., "Two-Dimensional CFD Modeling of Wave Rotor Flow Dynamics," *Proc. of the 11th AIAA Comp. Fluid Dynamics Conf.*, Pt. 1, AIAA-93-3318-CP, Orlando, FL, July, 6-9, 1993, pp. 234-247; also NASA TM-106261, 1993.

[14]Welch, G. E., "Two-Dimensional Computational Model for Wave Rotor Flow Dynamics," *J. of Engineering for Gas Turbines and Power*, **119**, No. 4, Oct., 1997, pp. 978-985.

[15]Paxson, D. E. and Lindau, J. W., "Numerical Assessment of Four-Port Through-Flow Wave Rotor Cycles with Passage Height Variation," AIAA-97-3142, July, 1997; also NASA TM-107490, June, 1997.
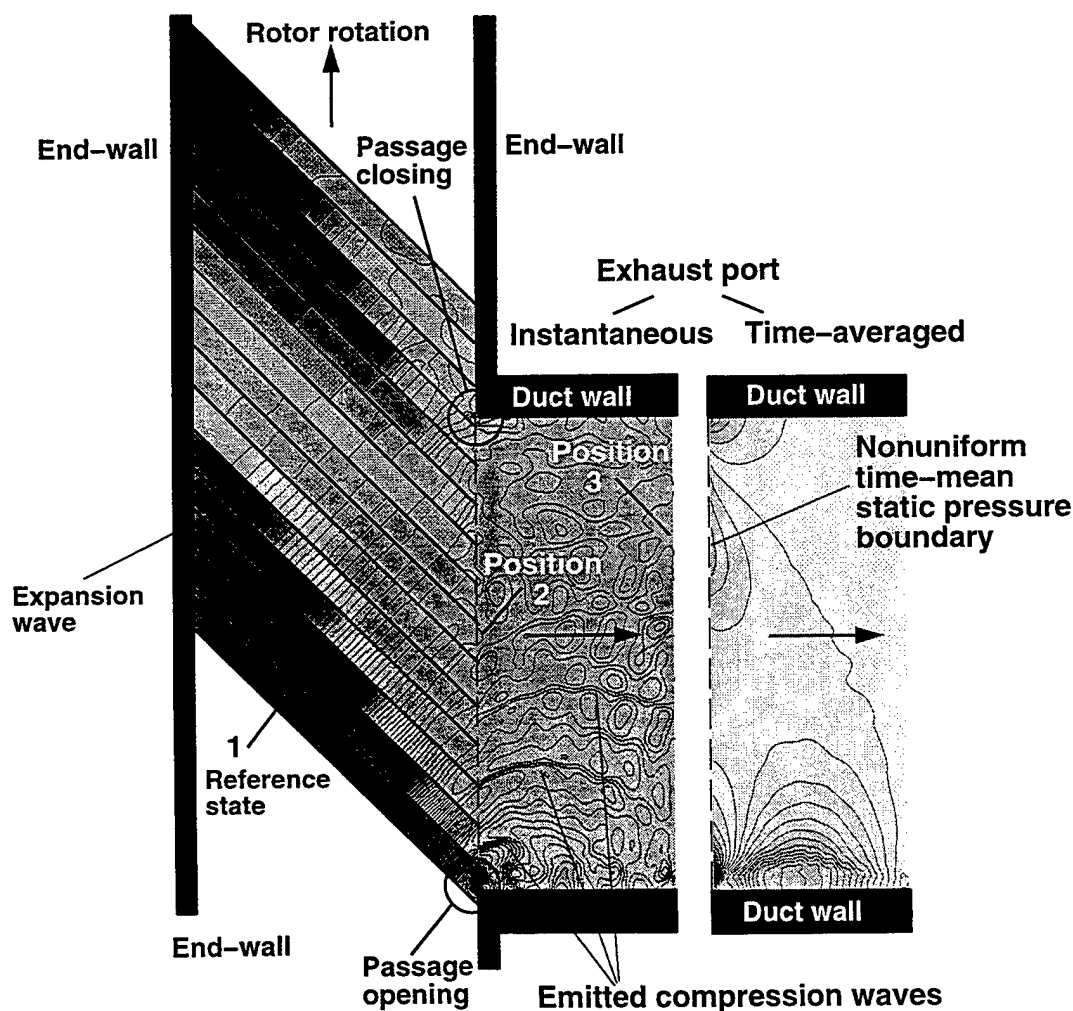
Figure 1. Schematic diagram of prototypical exhaust-port discharge problem comparing computed instantaneous and time-averaged static pressure contours.
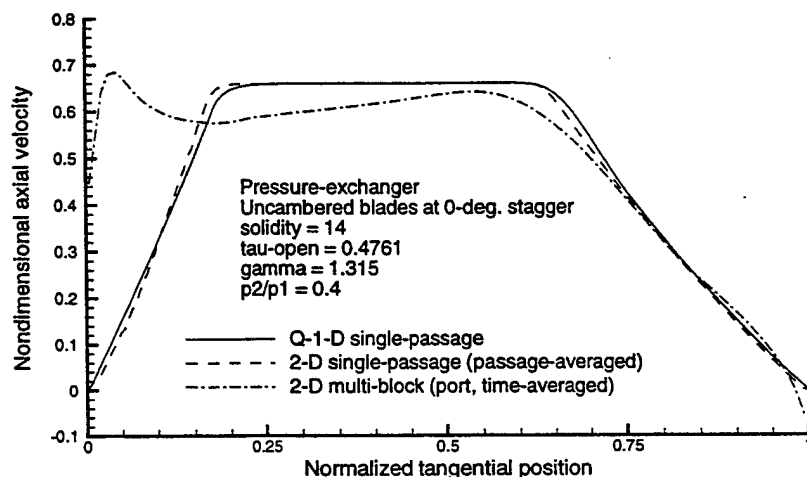
Figure 2. Comparison of computed nondimensional axial velocity as a function of normalized tangential position at the inlet of exhaust port of pressure–exchanger (0–degree stagger angle, zero–degree camber angle).
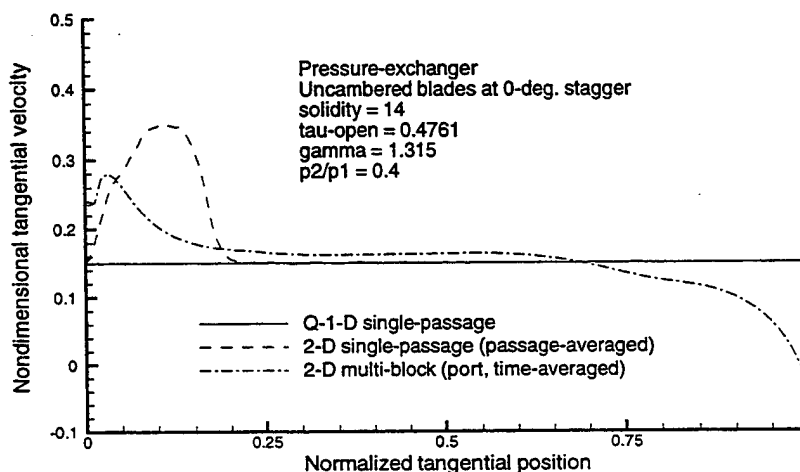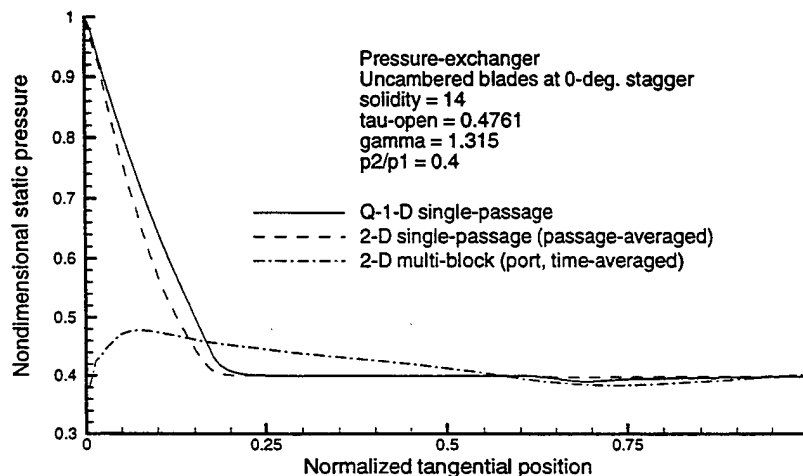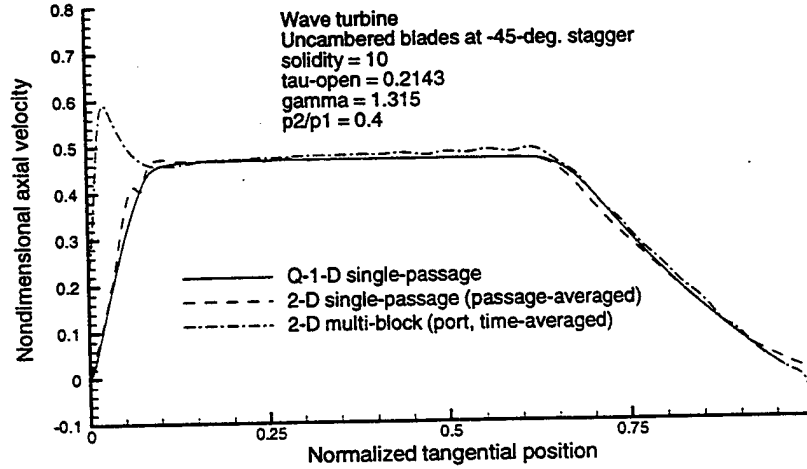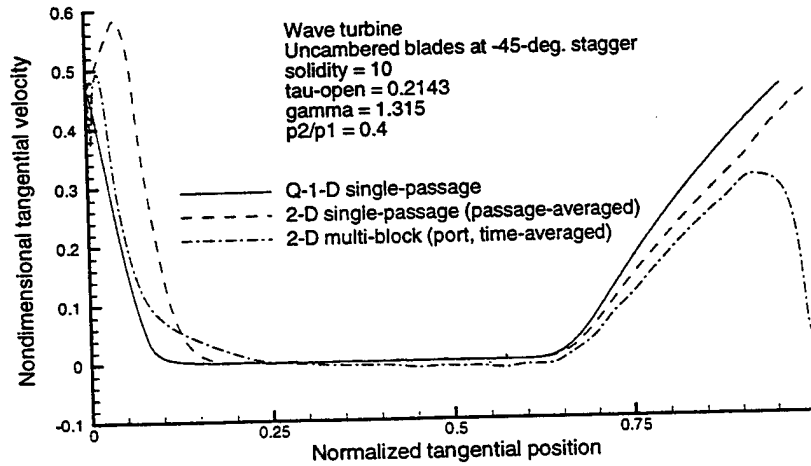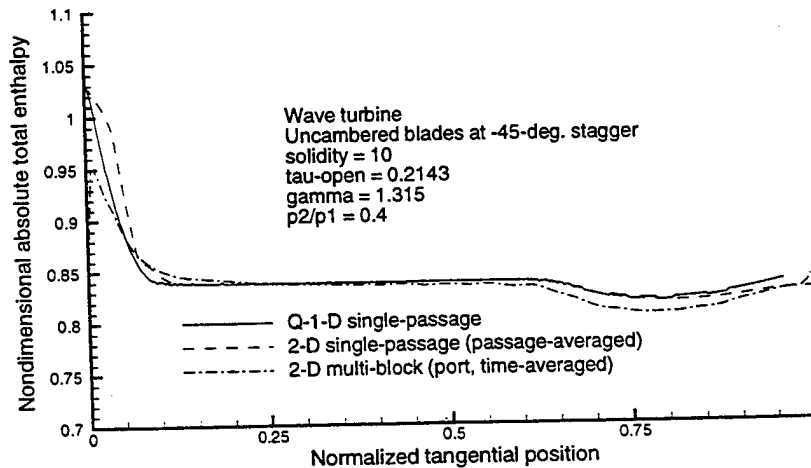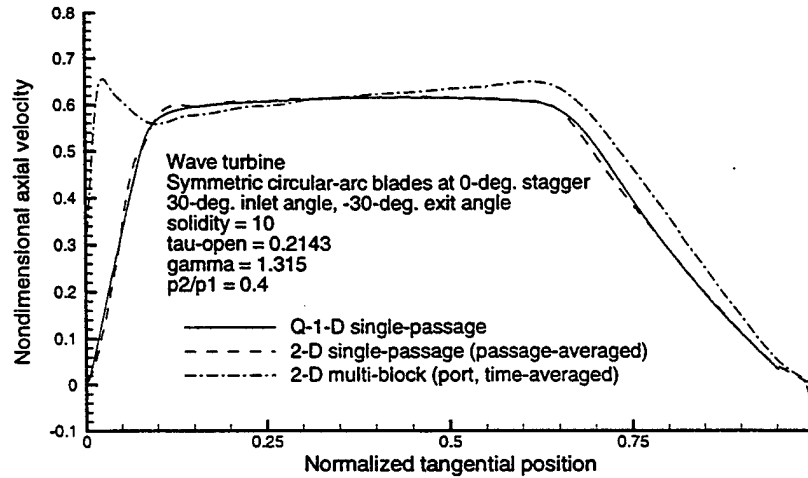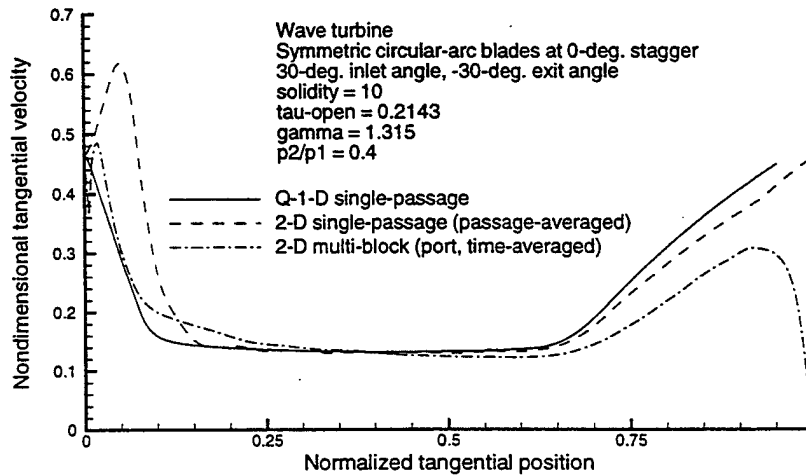

Figure 3. Comparison of computed nondimensional tangential velocity as a function of normalized tangential position at the inlet of exhaust port of pressure–exchanger (0–degree stagger angle, 0–degree camber angle).

Figure 4. Comparison of computed nondimensional static pressure as a function of normalized tangential position at the inlet of exhaust port of pressure–exchanger (zero–degree stagger angle, zero–degree camber angle).

10

Figure 5. Comparison of computed nondimensional axial velocity as a function of normalized tangential position at the inlet of exhaust port of wave turbine (−45−degree stagger angle, 0−degree camber angle).

Figure 6. Comparison of computed nondimensional tangential velocity as a function of normalized tangential position at the inlet of exhaust port of wave turbine (−45−degree stagger angle, 0−degree camber angle).
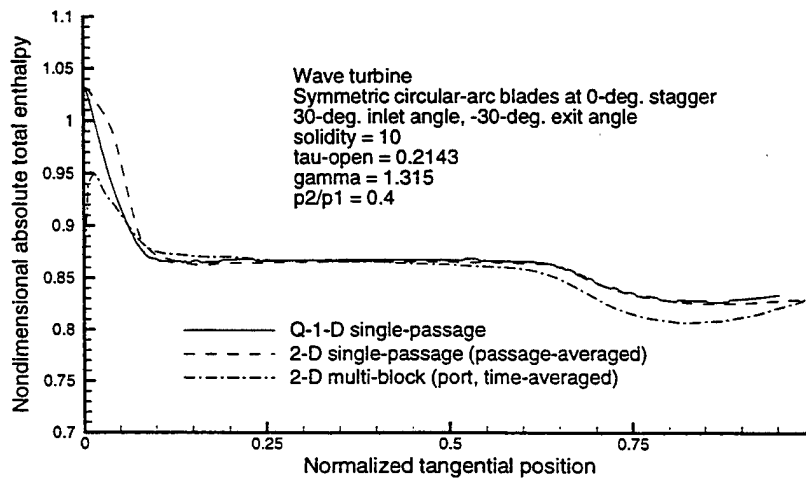

Figure 7. Comparison of computed nondimensional absolute total enthalpy as a function of normalized tangential position at the inlet of exhaust port of wave turbine (−45−degree stagger angle, 0−degree camber angle).

11

Figure 8. Comparison of computed nondimensional axial velocity as a function of normalized tangential position at the inlet of exhaust port of wave turbine with symmetric circular–arc blades (0–degree stagger angle, 60–degree camber angle).
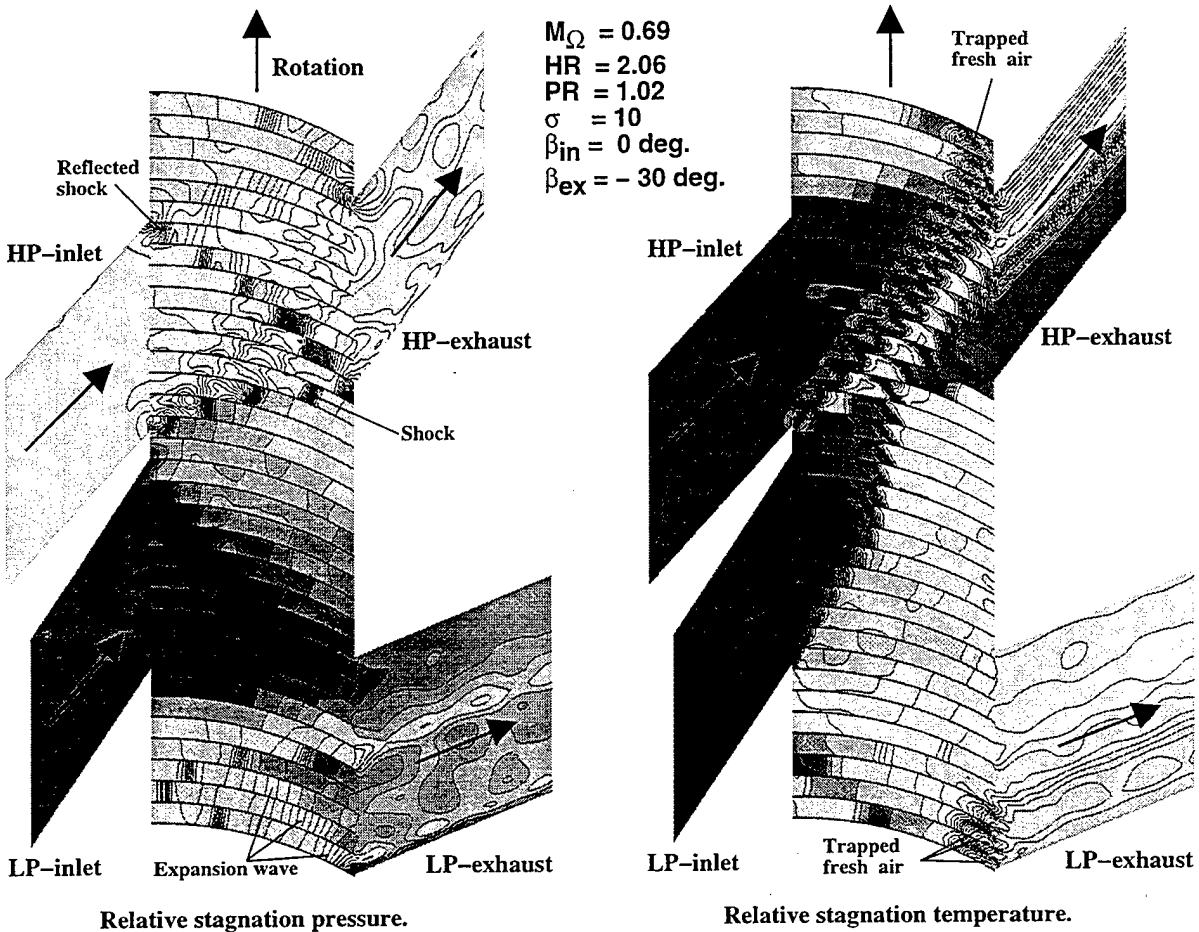

Figure 9. Comparison of computed nondimensional tangential velocity as a function of normalized tangential position at the inlet of exhaust port of wave turbine with symmetric circular–arc blades (0–degree stagger angle, 60–degree camber angle).

Figure 10. Comparison of computed nondimensional absolute total enthalpy as a function of normalized tangential position at the inlet of exhaust port of wave turbine with symmetric circular–arc blades (0–degree stagger angle, 60–degree camber angle).

$M_\Omega = 0.69$
$HR = 2.06$
$PR = 1.02$
$\sigma = 10$
$\beta_{in} = 0$ deg.
$\beta_{ex} = -30$ deg.

Relative stagnation pressure.

Relative stagnation temperature.

Figure 11. Instantaneous relative total pressure and relative total temperature contours in a four–port through–flow wave turbine computed by the 2–D multi–block solver.
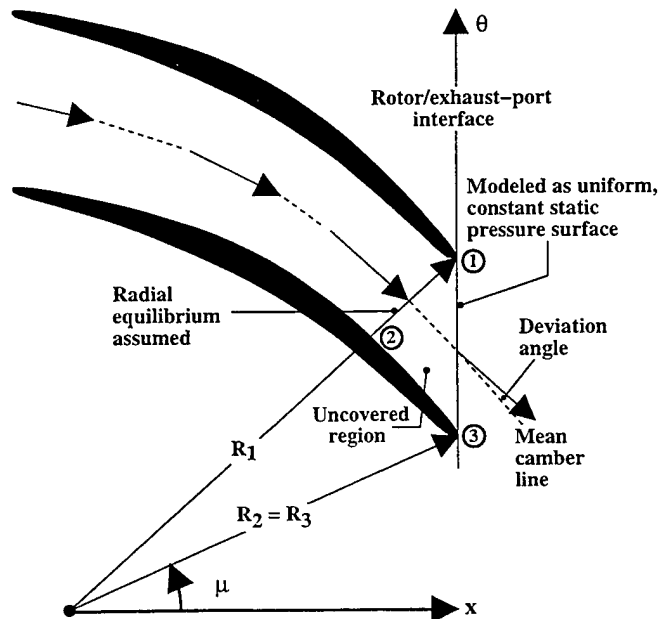

Figure 12. Schematic diagram for sub–model of inviscid flow deviation at trailing edge of a rotor passage.

REPORT DOCUMENTATION PAGE

1. AGENCY USE ONLY (Leave blank)	2. REPORT DATE July 1998	3. REPORT TYPE AND DATES COVERED Technical Memorandum

4. TITLE AND SUBTITLE

Wave Turbine Analysis Tool Development

6. AUTHOR(S)

Gerard E. Welch and Daniel E. Paxson

5. FUNDING NUMBERS

WU–523–26–33–00
1L161102AH45

7. PERFORMING ORGANIZATION NAME(S) AND ADDRESS(ES)

NASA Lewis Research Center
Cleveland, Ohio 44135–3191
and
U.S. Army Research Laboratory
Cleveland, Ohio 44135–3191

8. PERFORMING ORGANIZATION REPORT NUMBER

E–11261

9. SPONSORING/MONITORING AGENCY NAME(S) AND ADDRESS(ES)

National Aeronautics and Space Administration
Washington, DC 20546–0001
and
U.S. Army Research Laboratory
Adelphi, Maryland 20783–1145

10. SPONSORING/MONITORING AGENCY REPORT NUMBER

NASA TM—1998-208485
ARL–TR–1740
AIAA–98–3402

11. SUPPLEMENTARY NOTES

12a. DISTRIBUTION/AVAILABILITY STATEMENT

Unclassified - Unlimited
Subject Categories: 02 and 07   Distribution: Nonstandard

This publication is available from the NASA Center for AeroSpace Information, (301) 621–0390.

12b. DISTRIBUTION CODE

13. ABSTRACT (Maximum 200 words)

A quasi–one–dimensional (Q–1–D) computational fluid dynamic solver, previously developed and validated for pressure–exchanger wave rotors, is extended in the present work to include the blade forces of power producing wave rotors (i.e., wave turbines). The accuracy of the single–passage Q–1–D solver is assessed relative to two two–dimensional solvers: a single–passage code and a multi–block stator/rotor/stator code. Comparisons of computed results for inviscid, steady and unsteady flows in passage geometries typical of wave rotors reveal that the blade force model is accurate and that the correlation (effective stress and heat flux) terms of the Q–1–D passage–averaged formulation can be neglected. The ends of the rotor passages pose particular challenges to Q–1–D formulations because the flow there must at times deviate significantly from the mean camber line angle to match the port flow fields. This problem is most acute during the opening and closing of the rotor passages. An example sub–model is developed to account for the deviation between the flow departure angle and the mean camber line exit angle that occurs as an inviscid flow decelerates to meet a uniform pressure boundary. Comparisons of results from four–port wave turbine simulations reveal that the Q–1–D solver currently overpredicts wave turbine performance levels and highlight the need to devote future effort to the boundary conditions and sub–models of the Q–1–D solver.

14. SUBJECT TERMS

Gas turbine engine; Wave rotor; Wave turbine; Computational fluid dynamics; Pressure-exchanger; Simulation

15. NUMBER OF PAGES

19

16. PRICE CODE

A03

17. SECURITY CLASSIFICATION OF REPORT	18. SECURITY CLASSIFICATION OF THIS PAGE	19. SECURITY CLASSIFICATION OF ABSTRACT	20. LIMITATION OF ABSTRACT
Unclassified	Unclassified	Unclassified	